Tumor immunophenotyping-derived signature identifies prognosis and neoadjuvant immunotherapeutic responsiveness in gastric cancer

Jia-Bin Wang
Fujian Medical University Union Hospital
Qing-Zhu Qiu
Fujian Medical University Union Hospital
Qiao-Ling Zheng
Fujian Medical University Union Hospital
Ya-Jun Zhao
West District of the First Affiliated Hospital of USTC, University of Science and Technology of China
Yu Xu
The First Affiliated Hospital of Kunming Medical University
Tao Zhang
Liaoning Cancer Hospital & Institute, Cancer Hospital of China Medical University
Shuan-Hu Wang
The First Affiliated Hospital of Bengbu Medical College
Quan Wang
The First Hospital of Jilin University
Qin-Wen Jin
Guangxi Medical University Affiliated Tumor Hospital
Yin-Hua Ye
Fujian Medical University Union Hospital
Ping Li
Fujian Medical University Union Hospital
Jian-Wei Xie
Fujian Medical University Union Hospital
Jian-Xian Lin
Fujian Medical University Union Hospital
Jun Lu
Fujian Medical University Union Hospital
Qi-Yue Chen
Fujian Medical University Union Hospital

Long-Long Cao
Fujian Medical University Union Hospital
Ying-Hong Yang
Fujian Medical University Union Hospital
Chao-Hui Zheng
Fujian Medical University Union Hospital
Chang-Ming Huang (hcmlr2002@163.com)
Fujian Medical University Union Hospital

Research Article

Keywords: Gastric Cancer, Neoadjuvant Immune Checkpoint Inhibitor Therapy, Prognosis, Tumor Microenvironment, Immune Contexture.

Posted Date: November 10th, 2022

DOI: https://doi.org/10.21203/rs.3.rs-2248043/v1

Abstract

Background

The effectiveness of neoadjuvant immune checkpoint inhibition (ICI) therapy has been confirmed by clinical trials; however, patients that are suitable for receiving this therapy remain unspecified. Previous studies have demonstrated that the tumor microenvironment (TME) dominates immunotherapy; therefore, an effective classification strategy for the TME is needed.

Methods

Five publicly available datasets (n = 1,426) were used to identify the immunophenotypic features of the TME and to screen for core molecules. The training cohort (n = 506) was used to construct the immunophenotypic score (IPS) and six independent external centers (n = 638) were recruited as validation. Besides, 52 patients with GC receiving neoadjuvant anti-PD-1 therapy was enrolled to explore the value of the IPS in neoadjuvant ICI therapy. Moreover, the IPS-specific TME was profiled by multiplexed immunohistochemical staining and immunohistochemical staining.

Results

Five immunophenotype-related features (WARS, UBE2L6, GZMB, BATF2, and LAG-3) associated with prognosis and the immunotherapeutic response in GC were identified, forming the IPS. The data from seven medical centers (n = 1,144) indicated that the IPS is a robust and independent biomarker for GC and superior to the traditional TNM stage. Furthermore, IPS^{Low} was defined as the immune-activated tumor that benefited from neoadjuvant anti-PD-1 therapy, while IPS^{High} exhibited more immune unresponsive signals. Notably, patients with IPS^{Low} and PD-L1 (CPS) ≥ 5 were observed to be the most favorable group for neoadjuvant anti-PD-1 treatment.

Conclusions

The IPS could serve as a valid quantitative tool for immunophenotyping to improve clinical outcomes, and it provides an effective reference for the implementation of neoadjuvant ICI therapy for patients with GC.

Introduction

Immune checkpoint inhibitors (ICIs) have emerged as a revolutionary approach for significantly improving cancer immunotherapy outcomes by targeting immune checkpoints [1]. In the field of gastrointestinal tumors, many studies have reported the safety and efficacy of immune checkpoint

therapy [2]. In the phase III KEYNOTE-062 study, a monoclonal anti-PD-1 antibody showed single-agent activity in patients with advanced gastric cancer (GC) with microsatellite instability-high (MSI-H) [3]. The anti-PD-1 antibody significantly improved progression-free survival irrespective of PD-L1 expression in the ATTRACTION-4 trial [4]. Additionally, it showed an improvement in the overall survival (OS) of patients with a combined positive score (CPS) ≥ 5 combined with standard chemotherapy in the global CheckMate-649 trial and ORIENT-16 conducted in China [5, 6]. Thus, immunotherapy serves as the first line of treatment for GC [7], and a series of biomarkers represented by PD-L1 have shown significant advantages in advanced or metastatic GC, but the effect of treatment in resectable GC remains unknown.

Neoadjuvant immunotherapy provides a potential treatment strategy when the tumor may be curable. Notably, more than 100 clinical trials of neoadjuvant anti-PD-(L)1 blockade (as monotherapy or combination therapy) are ongoing or planned for various tumor types [8]. In the GERCOR NEONIPIGA phase II study, neoadjuvant therapy with anti-PD-1 therapy resulted in a complete pathological response in nearly 60% of patients with esophagogastric adenocarcinoma with MSI/dMMR [9] demonstrating that neoadjuvant therapy is not only effective but also may lead to patients' cure. Encouragingly, in another small phase II clinical trial, 12 patients with rectal cancer received innovative PD-1 blockade immunotherapy, and their tumors disappeared without follow-up chemotherapy, radiation, or surgery [10]. Neoadjuvant immunotherapy enhances systemic antitumor immunity and immune surveillance after surgery [11]. Thus, it is necessary to screen patients suitable for neoadjuvant immune checkpoint therapy, which may be superior or complementary to existing treatment options.

Currently, the benefits of immune checkpoint blockade therapies depend largely on the status of the TME, of which T cells are the most important as antitumor executors. Some studies have classified tumors into immune-inflamed, -desert, and -excluded phenotypes based on the spatial localization of immune cells relative to the tumor and stromal compartments [12]. Inflamed tumors may be more likely to respond to immune interventions to counteract the tumor-induced T cell dysfunction, while non-inflamed tumors may require novel targeted therapies to induce T cell activation and migration due to the lack of tumor-infiltrating T cells [13, 14]. The ultimate efficacy of immunotherapy is mainly determined by the antitumor immune response shaped by the complex interactions among diverse components in the TME. $CD8^+$ T cells can cause tumor cell death by producing perforin, granzyme, etc. [15]. $CD8^+$ T cells can also express high levels of co-inhibitory receptors, such as PD-1, CTLA-4, and LAG-3, to shrink the ongoing T cell response but are exploited by tumors to suppress antitumor responses [16]. Blocking signaling of the immune checkpoints can improve $CD8^+$ T cell responses, and dual immune checkpoint blockade appears to better enhance T cell expansion and function [17–20].

Presently, the dominant role of the TME in affecting the immunotherapeutic response has been confirmed [21]. It is crucial to identify immunophenotypes of the immunotherapy response in the TME to enhance antitumor immunity and improve clinical outcomes. Although MSI/TMB-based staging is available in GC, its ability to guide GC immunotherapy, especially neoadjuvant immunotherapy, needs to be further enhanced. Consequently, it is necessary to find new and more comprehensive immunophenotyping to guide GC immunotherapy based on the TME. This study aimed to search for immunophenotypes in the

TME associated with immunotherapy responsiveness. The goal was to construct simple and reliable TME signature-derived immunophenotyping for patients with GC to delineate the immune context, reveal prognostic information, and predict the ICI treatment response. Unlike previous studies, the results of the present study can be used to guide neoadjuvant immunotherapy and help surgeons select more favorable neoadjuvant immunotherapy regimens for patients with GC based on the immunophenotype.

Materials And Methods

Study design and data sources

In this multicenter, retrospective study, genomic data and clinicopathological information on 1,426 patients with GC from five publicly available GC datasets were obtained, and 1,326 patients with GC were enrolled from seven independent medical centers in different geographic regions of China (Fig. 1a).

To identify potential genes that classify the TME, all gene expression data and clinicopathological information of TCGA-STAD, ACRG/GSE66229, GSE84433, GSE26942, and GSE15459 were obtained from The Cancer Genome Atlas (TCGA) and Gene Expression Omnibus (GEO). The R software (version 3.6.3) package 'Affy' was used for the raw dataset data from Affymetrix to execute the background adjustment [22]. The 'lumi' package was used in the raw dataset data from Illumina. The 'ComBat' algorithm was used to reduce the likelihood of batch effects from non-biotech biases.

To construct and explore the TME-based immunophenotype score (IPS), formalin-fixed paraffin-embedded (FFPE) specimens of 687 patients with GC from Fujian Medical University Union Hospital (FMUUH, Fuzhou, China) were included. A total of 506 patients without neoadjuvant treatment who underwent D2 GC radical surgery from 2012 to 2015 were enrolled to construct and validate the prognostic value of the IPS, of which 253 were used to characterize the immune microenvironment. A total of 638 GC tissues and clinicopathological specimens collected between September 2008 and March 2016 from six external centers were used to test the prognostic value of the IPS. Among these, 98 cases were from the Liaoning Cancer Hospital & Institute (LCH, Shenyang, China), 96 were from the Bethune First Affiliated Hospital of Jilin University (JUBFAH, Changchun, China), 97 were from the First Affiliated Hospital of Bengbu Medical College (BMCFAH, Bengbu, China), 181 were from the First Affiliated Hospital of the University of Science and Technology of China (USTCFAH, Hefei, China), 60 were from the Guangxi Medical University Affiliated Tumor Hospital (GMUATH, Nanning, China), and 106 were from the First Affiliated Hospital of Kunming Medical University (KMUFAH, Kunming, China). As illustrated in Fig. 1a, the six independent medical centers were combined into three cohorts based on their geographical location. Clinicopathological information of patients with GC enrolled in these cohorts is listed in **Supplementary Table S1** and **S2**. The inclusion and exclusion criteria for patients were as follows: (1) histological identification of GC, (2) no other malignant tumors or distant metastases, (3) availability of follow-up data and clinicopathological characteristics, and (4) TNM staging of GC tumors according to the 2010 International Union Against Cancer guidelines. The exclusion criteria were as follows: (1) death within 1 month of surgery and (2) chemotherapy or radiotherapy before surgery. All participants with advanced GC

routinely received fluorine-based chemotherapy. The patient follow-up strategy is available in our previous study (2). Informed consent was obtained from all participants.

To explore the genomic features of the IPS, 79 patients who underwent D2 GC radical surgery at FMUUH from 2017 to 2021 were included. Of these, 47 were commissioned to Novogene Co., Ltd. (Beijing, China) for whole-exome and whole-transcriptome sequencing, and 32 were sequenced by Kangchen Biotechnology Co., Ltd. (Shanghai, China) for whole-transcriptome sequencing. Whole-exome sequencing was performed in Illumina HiSeq PE150 using Agilent SureSelect Human All Exon V5/V6 (Agilent Technologies, CA, USA). Whole transcriptome sequencing was performed on the Illumina HiSeq platform using TruSeq SR Cluster Kit v3-cBot-Hs (Illumina, CA, USA). After removing batch effects by the 'ComBat' algorithm, the FMUUH_RNA-Seq cohort was combined from the sequencing data analyzed by the two companies. The clinical characteristics of these patients are listed in **Supplementary Table S3**.

To identify the value of the IPS to predict neoadjuvant immunotherapy, 167 locally advanced patients with GC who received neoadjuvant therapy at the FMUUH from March 2019 to November 2021 were included, of which 63 were excluded due to the limited area of the tumor region or a lack of biopsy specimens, and 104 were finally included, whose baseline information is shown in **Supplementary Table S4**. All patients received a chemotherapy regimen based on fluorouracil and nab-paclitaxel. Of these, 52 with the addition of anti-PD-1 therapy (camrelizumab) were enrolled into the neoadjuvant immunotherapy cohort. The remaining 52 who received chemotherapy alone were classified as the neoadjuvant chemotherapy cohort. Their specific treatment regimens and inclusion criteria are detailed in our previous study [23]. For the efficacy evaluation, the effect of neoadjuvant therapy was evaluated independently by two specialized radiologists following the guidelines of the Response Evaluation Criteria in Solid Tumors (RECIST version 1.1) [24], and the final results were determined after a cross-review of the results. For the evaluation of postoperative pathological tissue, the tumor regression grade (TRG) was determined according to the Becker criteria [25, 26]. The pathologic complete response (pCR) was defined as the absence of invasive disease, and total lesions and histologically negative lymph nodes were evaluated. The overall design flow of this study is shown in Fig. 1b.

The ethics approval number for this research project is 2022KY084 and was obtained from the FMUUH. All seven centers approved this study and all patients signed informed consent forms before tissue collection.

Consensus Clustering Of Immune Phenotypes

The immune cell ratios of GC tissue were quantitated using the CIBERSORT algorithm and LM22 gene signature [27]. Then, the package 'ConsensuClusterPlus' [28] was applied to perform hierarchical agglomerative clustering (based on the Euclidean distance and Ward's linkage) of the infiltration of five types of immune cells (CD8, memory CD4, and resting memory CD4 T cells; M1 and M2 macrophages), applying an unsupervised clustering (K-means) approach to identify and classify patients with different

immune phenotypes. In this case, a consensus clustering algorithm with 1,000 iterations was used to determine the optimal number of clusters (k = 3).

Identification Of Immunophenotype-associated Differentially Expressed Genes (Degs)

The R package 'limma' was used to identify immunophenotype-associated DEGs [29]. Meanwhile, to rank the importance of DEGs for the immunophenotype in the five GC datasets (TCGA-STAD, ACRG/GSE66229, GSE84433, GSE26942, and GSE15459) and to reduce the bias caused by the unequal number of cases in each dataset, a formula was constructed to calculate the weight of each DEG:

$$\mathrm{Weight} = \sum \left(\mathrm{LogFC} \times \frac{2}{(1 + \mathrm{adj.}\, p\mathrm{value}} \times (\mathrm{AUC} - 0.5) \times \mathrm{Log2}\,(\mathrm{HR}) \times \left(\frac{\mathrm{n}_i}{\mathrm{N}} \right) \right)$$

This weight was calculated as the DEGs between IMcluster A and IMcluster B/C. AUC is the area under the ROC curve predicting IMcluster A; HR is the hazard ratio to prognosis in the Cox regression model; n_i is the number of patients in the individual dataset; N is the sum of cases in the five GC datasets.

Immunohistochemistry Staining And Evaluation

Immunohistochemistry was applied to 4 μm-thick FFPE GC tissue, as described in previous studies. Details of the primary antibodies are shown in **Supplementary Table S5**. The Motic EasyScan system (Motic, Xiamen, China) and Nikon E200 (Nikon, Tokyo, Japan) microscope were used to acquire images.

For the staining of immunophenotype-associated DEGs, DEGs were quantified by the H-score:

$$\text{H-Score} = (1 \times \text{Weak Stain \%}) + (2 \times \text{Medium Stain \%}) + (3 \times \text{Strong Stain \%})$$

The Immunohistochemical scoring criteria (WARS, UBE2L6, GZMB, BATF2, and LAG-3) is illustrated in **Supplementary Fig. S1a.**

Four mismatch repair proteins (MSH2, MSH6, MLH1, and PMS2) were employed to determine MSI status. The scoring criteria (**Supplementary Fig. S1b**) were at least one missing mismatch repair gene-related protein, interpreted as deficient mismatch repair (dMMR), manifested as microsatellite instability (MSI)-H; no missing mismatch repair gene-related protein was interpreted as proficient MMR, manifested as MSI-L/MSS. The Epstein–Barr virus (EBV) status was measured by in situ hybridization using an EBER probe (ISH-6021, ZSGB-BIO, China; **Supplementary Fig. S1b**).

To assess the infiltration of immune cells, five representative 200× fields of view were acquired in the core of tumor (CT) and invasive margin (IM) of each GC tissue to calculate the positive cell density (**Supplementary Fig. S1c**):

$$\text{Density} = \frac{C_{P1} + C_{P2} + C_{P3} + C_{P4} + C_{P5}}{Area_1 + Area_2 + Area_3 + Area_4 + Area_5}$$

C_{Px} is the total number of cells stained as positive in this field; $Aare_x$ is the area of this field. The positive cell count was assisted by the Measurement plugin of Image Pro Plus software (version 6.0, Media Cybernetics, USA), which was also used to determine the area of the tumor region. The Inflamed, Excluded, and Desert phenotypes were determined based on immunohistochemical staining slides for $CD8^+$, and these three immunophenotypes were classified based on the characteristics reported in previous studies. PD-L1 expression was measured by using the CPS:

$$\text{CPS} = \frac{\text{total number of positive stain cells for PD-L1}}{\text{total number of viable tumor cells}} \times 100$$

Positive stain cells for PD-L1 included PD-L1-expressing tumor cells, lymphocytes, and macrophages.

Two senior pathologists, blind to the clinicopathological features and prognosis of the patients, scored all samples independently. For the assessment of immunophenotype-related DEGs, 74.7% of the samples were scored in complete agreement, and 23.8% differed by 10% or less. The two pathologists were in complete agreement on the determination of MSI and EBV status. When the difference between the scores scored by the two independent pathologists was within 10%, the average of the two was taken; when the difference was greater than 10%, a third pathologist reviewed the results and selected one of the scores from the first two pathologists, or the three pathologists reached consensus.

Construction Of The Ips

The Least Absolute Shrinkage and Selection Operator (LASSO) Cox and randomSurvivalForest algorithms were used to identify immunophenotype-associated DEGs associated with GC prognosis. In the LASSO Cox model, Lambda (− 4.2503), selected by the least deviation likelihood ratio, failed to exclude any of the eight genes. RandomSurvivalForest was simultaneously run. Interestingly, the five genes that were included when considering the importance of 0.03 as the threshold were the same as those included in the LASSO analysis when the Lambda was − 2.2966. The ROC curves corresponding to the two Lambdas were compared, and it was found that the AUC decreased by only 0.01 after excluding three genes, and this sacrifice was acceptable for improving the simplicity of using the model; thus, these five genes (*GZMB, WARS, LAG-3, BATF2, and UBE2L6*) were included in the final model construction. To reduce bias in model construction, specimens of the remaining 253 patients with GC in the Training Cohort were also stained for the five genes. Next, a multivariate Cox proportional hazards regression with a stepwise procedure was performed to obtain predictive models based on immunophenotype-related DEGs, and risk scores for each patient were obtained using the R package ‘survival’. Since the scoring model was constructed based on the immunophenotype, the risk score was named the IPS. The ‘ggrisk’ package was used to determine the Youden index of the risk score and classify patients into low risk (IPS^{Low}) and high risk (IPS^{High}) groups depending on this score.

Multiplex Immunohistochemistry Staining

The Opal 7-color Kit (NEL871001KT, Akoya Bioscience, USA) was used to perform multiplex immunohistochemistry staining to identify macrophages M1 and M2 (CD68/CD163/CD206/INOS). Effector T cells (Teffs; GZMB/CD8) were characterized separately in two separate panels using the Opal 4-color Kit (NEL840001KT, Akoya Bioscience, USA). Labeling of multi-cytokeratin using panCK (ab7753, Abcam, UK) in all panels was used to segment tumor-nest and stroma or to determine IM. The nuclei of all cells were stained by DAPI (D9542, Sigma-Aldrich, USA). Details of the primary antibodies are displayed in **Supplementary Table S5**.

The Mantra System (PerkinElmer, USA) was applied to capture multispectral panoramic images after staining. The scanned slides were then analyzed by InForm software (PerkinElmer, USA) to obtain quantitative data on the region of interest (ROI). InForm can accurately count the positive cells and identify them by setting reasonable thresholds, which allows for the computation of the density and ratio of the target cells in the ROI. It also allows automated segmentation of the tumor-nest ($panCK^+$) and stroma ($panCK^-$) to collect quantitative data from different ROIs.

Statistical analysis

The LASSO regression model was analyzed by the R package 'glmnet', while randomSurvivalForest was constructed by the practical R package 'randomForestSRC'. The Mann–Whitney U-test was carried out to compare two groups of non-normally distributed continuous variables, while the Kruskal–Wallis test was used to perform multiple comparisons. Categorical variables of clinicopathological characteristics were compared using the χ^2 test or Fisher's exact test. Nonparametric correlation analyses were performed using Spearman's test. Kaplan–Meier survival analysis with log-rank test was used to estimate OS. The univariate Cox proportional hazard regression model was used to confirm the association between the relevant clinicopathological variables and OS. Next, multivariate Cox regressions were included to analyze indicators that were statistically significant ($p \leq 0.05$) in the univariate analysis (Training Cohort: IPS, tumor size, degree of differentiation, pTNM stage, CEA, and CA19-9; Central China Cohort: IPS, degree of differentiation, pTNM stage; North China Cohort: IPS and pTNM stage; South China Cohort: IPS, degree of differentiation, and pTNM stage). Univariate and multivariate logistic regression was used to determine the association of variables with response to immunotherapy.

Results

Construction of an immunophenotype-based signature

In this exploratory study, we processed the gene expression profiles of 1426 gastric cancer (GC) patients using bioinformatics algorithms to identify 3 clusters of prognosis- and immune checkpoint-related immunophenotypes in tumor microenvironment (TME) (**Supplementary Fig. S2a-b**). IMcluster A exhibited immune activation, characterized by hyper-expression of CD8 T cells, memory CD4 T cells, and M1

macrophages (**Supplementary Fig. S2c-d**). By Kaplan–Meier survival analysis, it was observed that IMcluster A was associated with improved prognosis for patients with GC (**Supplementary Fig. S2e**). Meanwhile, in two online available datasets receiving ICIs therapy (IMviogr210 and GSE91061), patients in IMcluster A were observed to be more responsive to ICI therapy (**Supplementary Fig. S3)**. Overall, the publicly available dataset supported that IMcluster A represented a well-prognosed and immunotherapy-sensitive immunophenotype.

Construction Of An Immunophenotype-based Signature Applicable To Pathological Tissues

Respective weights were assigned to the 497 differential expressed genes (DEGs; IMcluster A vs IMclusterB/C) screened by the 'limma' package. Based on the weight ranking, the top 30 DEGs in weight ranking were selected as the major immune activation genes (**Supplementary Fig. S4a**). Currently, in addition to gene expression profile-based signatures, high-accuracy pathological tissue-applicable models have high detection convenience and predictive accuracy. However, IMcluster was determined based on the transcriptional level, whereas immunohistochemical staining applicable to pathological tissues is a tool to detect the translational level. To determine whether these immune activation genes screened by transcriptional level can be used for immunohistochemical detection, transcriptome sequencing was performed to obtain mRNA expression profiles of the top 30 DEGs in 79 gastric adenocarcinoma tissues from our center. Meanwhile, the pathological tissues of these 79 patients with the top 30 DEGs were stained using immunohistochemistry, and the correlation between the transcriptional and translational levels of each gene was calculated by Spearman's test (**Supplementary Fig. S4b**). Eight of the top 30 DEGs (*GZMB, WARS, LAG-3, ETV7, BATF2, PSMB9, PSMB10, and UBE2L6*) were finally selected according to the *p*-value.

Immunohistochemical staining of these eight genes was performed in the Discovery Cohort (**Supplementary Fig. S5a**). By using LASSO Cox and RandomSurvivalForest algorithm, five molecules (GZMB, WARS, LAG-3, BATF2, and UBE2L6) were finally screened that were strongly associated with the prognosis of GC. Next, a proportional risk regression model based on 5 indicators, called Immunophenotypic score (IPS), was constructed. Patients with GC were classified into low-risk (IPS^{Low}) and high-risk (IPS^{High}) groups according to their risk score. The detailed steps of the process are described in **Methods**.

Characterization Of The Transcriptome And Genome Of The Ips

Patients in the FMUUN_RNA-Seq cohort were the only ones for whom simultaneous evaluation of IMcluster and IPS was possible. By comparing the patient composition of IMcluster and IPS, it was found that 78.1% of IMcluster A patients were identified as IPS^{Low}, while IPS^{High} was mostly composed of IMcluster B with IMcluster C (**Supplementary Fig. S5f**). For IMcluster, the clustering results were consistent with those obtained from the five public datasets (**Supplementary Fig. S6a**). This identified

IPS^{Low} as having most of the features of IMcluster A, while IPS^{High} had the opposite. Due to hypothesizing that the biological properties of different IPSs may be very different, the transcriptomic and genomic features of the FMUUN_Seq cohort were analyzed. The GO enrichment analysis of the DEGs between IPS^{Low} and IPS^{High} revealed that genes implicated in immune activation were enriched in IPS^{Low} (**Supplementary Fig. S6b-c**). Similarly, GSEA analysis revealed that immune activation-, immunotherapeutic response-, antigen presentation-, and tumor-killing-related pathways were upregulated in IPS^{Low} (**Supplementary Fig. S6d**). Furthermore, whole-exome sequencing of 48 cases in the FMUUN_Seq cohort was performed simultaneously, and it was found that IPS^{Low} was consistent with significantly higher tumor mutations than IPS^{High} (**Supplementary Fig. S6e**). By analyzing mutation annotation files, mutated genes were also found to differ between IPS^{Low} and IPS^{High}, which may provide new perspectives on exploring the formation of immunophenotypic disparities (**Supplementary Fig. S6f**). In short, IPS^{Low} shares most of the overlap with IMcluster A. Meanwhile, transcriptomic and genomic profiles indicated that IPS^{Low} featured a higher tumor mutational load and was associated with immune activation and improved immunotherapeutic response.

Validation Of The Prognostic Presentation And Clinical Features Of The Ips

To further validate the performance of the IPS for clinical translation, the prognostic potential of the IPS was examined in the Training Cohort and three external cohorts consisting of GC patients from six external independent medical centers. Time-dependent ROC curves revealed a robust and stable discriminatory power of IPS in four independent cohorts (Fig. 2a-d). Previous studies reported that some clinical features (e.g., $AJCC_{8th}$ and differentiation) and molecular subtypes (MSI and EBV statuses) can also be used to evaluate the prognosis of patients with GC. Therefore, the efficacy of IPS was compared with other clinical features or molecular subtypes in predicting the prognosis. As shown in Fig. 2e-h, the predictive accuracy of the IPS was significantly superior to other variables, including $AJCC_{8th}$, age, sex, differentiation, MSI status, and EBV status. In addition, Kaplan–Meier survival analysis indicated that patients with IPS^{Low} had better OS compared to those with IPS^{High} in four independent cohorts (Fig. 2i-l). Stratified analysis based on $AJCC_{8th}$, differentiation, MSI status, and EBV status illustrated the same trend (**Supplementary Fig. S7a-d**). Notably, the lack of statistical significance for stage I in the Training Cohort and Central China Cohort and stage II in the North China Cohort may be attributed to the smaller sample size and lower mortality rates. Univariate and multivariate Cox regression analysis of multiple cohorts reconfirmed the prognostic value of the IPS, and both the IPS and $AJCC_{8th}$ were significant in multivariate Cox analysis, suggesting that the IPS coupled with AJCC is an excellent combination for predicting the prognosis (Fig. 2m and **n**). Furthermore, $\chi 2$ tests were used to determine the association between the IPS and clinicopathological features and molecular subtypes, and the results showed a significant correlation of IPS with $AJCC_{8th}$, MSI status, and EBV status (**Supplementary Table S6-7**). This

indicated that IPS^{Low} exhibited less lymph node metastasis and more muted tumor invasion (**Supplementary Fig. S8a-c**).

Overall, multicenter data supported the IPS as a robust prognostic biomarker for GC working independently of clinicopathologic features. Moreover, MSI-H and EBV-positive patients had a lower IPS, which could mean that the IPS is a potential surrogate for MSI or EBV statuses and that patients with hypo-IPS may exhibit partial MSI-H or EBV-positive features (**Supplementary Fig. S8d**). In previous studies, MSI-H and EBV positivity have been considered favorable features for immune infiltration and immunotherapeutic responses [10, 30, 31], which laterally reflects the potential of the IPS in immunotherapy. Notably, the aforementioned enrichment analysis indicated that the IPS is related to the activation of antitumor immunity and the immunotherapeutic response (**Supplementary Fig. S6c** and **d**). Therefore, it was hypothesized that the IPS could not only map MSI/EBV status but also more accurately reflect the immune status and response to immunotherapy.

Deconstructing The Immune Microenvironmental Landscape Of Ips Specificity

To unmask the IPS-specific immune microenvironment, several immune markers (including total $CD45^+$ leukocytes; total T leukocytes $CD3^+$, cytotoxic T leukocytes $CD8^+$, helper T leukocytes $CD4^+$, activated and memory T leukocytes $CD45RO^+$, and $FOXP3^+$regulatory T leukocytes) were first quantified in the core of tumor (CT) and invasive margin (IM) (**Fig. S1c** and **Supplementary S9a**). No distinction in total leukocyte ($CD45^+$) infiltration between IPS^{Low} and IPS^{High} tumors was observed (**Supplementary Fig. S9b**). Figure 3a and **Supplementary Figure S9c** indicated that in either the CT or IM, IPS^{Low} tumors exhibited more enriched infiltration of $CD3^+$, $CD4^+$, $CD8^+$, and $CD45RO^+$ compared to that in IPS^{High}. In contrast, $FOXP3^+$ showed more infiltration in IPS^{High} tumors. Meanwhile, Spearman's correlation analysis identified the same trends (**Supplementary Fig. S9d**). By comparing the infiltration of CT versus IM, it was discovered that $CD3^+$, $CD8^+$, and $CD45RO^+$ had a higher core-to-margin ratio (CT/IM) in IPS^{Low} tumors, which seemed to imply a more intensive infiltration of $CD3^+$, $CD8^+$, and $CD45RO^+$ from the IM toward the CT in IPS^{Low} tumors (Fig. 3b). $FOXP3^+$ tended to be silent in the CT of IPS^{Low} tumors. The infiltration distribution characteristics of the respective IPS fit the description of the previously reported three immunophenotypes (Inflamed, Excluded, and Desert). Therefore, the immunophenotypic composition of different IPSs was evaluated and compared (**Supplementary Fig. S9e**). As expected, 65.23% of tumors in IPS^{Low} were Inflamed tumors, which was significantly higher than the 18.84% in IPS^{High} ($\chi 2$; $p < 0.001$, Fig. 3c). In contrast, Excluded (33.33%) and Desert (47.82%) were more frequently found in tumors of IPS^{High}. The Kruskal–Wallis test reconfirmed that Inflamed had the lowest IPS (Fig. 3c). This may imply that the IPS reflects the spatial distribution characteristics of T cells to some extent. In addition, Teffs are critical for antitumor immunity as tumor-killing executors, and their marker, GZMB, is one of the components that constitute the IPS. Therefore, the association between Teffs and the IPS was investigated by characterizing Teffs in the tumor-nest versus the stroma using CD8A and GZMB (Fig. 3d

and **Supplementary S9f**). The findings indicated that IPS^{Low} tumors not only had an abundant infiltration of Teffs, but also concentrated Teffs in the tumor-nest, and this trend was more pronounced in the CT (Fig. 3e and **Supplementary S9g-h**). Meanwhile, a higher proportion of Teffs was observed in IPS^{Low} tumors and reached the maximum in the tumor-nest in the CT. In contrast, Teffs in IPS^{High} were localized to the stroma. These data suggest that IPS^{Low} was a subtype with a positive antitumor immune response.

The clustering basis of the IMcluster on which the IPS was developed contains M1- and M2-like macrophages. Therefore, the infiltration characteristics of TAMs from the diverse IPS tumors were also explored (Fig. 3f). Multiplex immunofluorescence staining demonstrated distinct infiltrative profiles of TAMs in IPS^{Low} versus IPS^{High} tumors, with IPS^{High} tumors showing a significant abundance of M2-like TAMs in both the CT and IM of the tumor compared to IPS^{Low} tumors (Fig. 3g and **h**). In contrast, in IPS^{Low} tumors, a more M1-like phenotype was observed in the CT (Fig. 3g and **h**). Although a trend was found for $CD68^+CD163^+$, $CD68^+CD163^+CD206^+$, and $CD68^+INOS^+$ in the IM, the results were not significant, which may be related to the limited sample size. Moreover, the distribution of each TAM phenotype in IPS^{Low} and IPS^{High} tumors, respectively, was explored. In IPS^{Low} tumors, the CT revealed an increased density of $CD68^+INOS^+$ M1-like TAMs compared to the IM, while $CD68^+CD206^+$ and $CD68^+CD163^+CD206^+$ M2-like TAMs tended to accumulate in the IM, with no discrepancy for $CD68^+CD163^+$ (Fig. 3i). For IPS^{High} tumors, aggregation in the CT on TAMs of $CD68^+CD163^+$ was observed, while the distribution of TAMs of CD206 was reversed (Fig. 3i). In conclusion, M1-like TAM levels were more intensive in the CT of IPS^{Low} tumors and decreased toward the IM, whereas M2-like ($CD68^+CD163^+$ and $CD68^+CD163^+CD206^+$) TAM levels were less dense and restricted to the tumor margins. In IPS^{High} tumors, TAMs displayed a more M2-like phenotype compared to in IPS^{Low} tumors, while $CD68^+CD163^+$ and $CD68^+CD163^+CD206^+$ M2-like TAMs accumulated in the CT and reduced towards the IM, and $CD68^+CD206^+$ M2-like TAMs dominated in the IM and reduced towards the CT.

Evaluation of the immune microenvironment indicated that the antitumor effect of the TME of IPS^{High} was muted with a significant inhibitory profile, which was defined as immune-silenced. Conversely, IPS^{Low} exhibited an immune-activated profile, which was considered a beneficial signal for immunotherapy [32–35]. Therefore, it was hypothesized that different levels of IPSs would respond diversely to immunotherapy.

The Ips Predicts Neoadjuvant Immunotherapeutic Benefits

Patients receiving neoadjuvant therapy have only biopsied tissue available for evaluation before treatment. In the present study, we demonstrated that IPS can be used for biopsy tissue that can be evaluated for tumor areas larger than 0.16 mm^2 (**Supplementary Fig. S10** and **Supplementary Methods**).

By evaluating the IPS of 52 patients who received anti PD-1 therapy, 25 were considered IPS^{Low} and 27 were IPS^{High} (Fig. 4a and **Supplementary S11a**). Encouragingly, more IPS^{Low} patients experienced tumor

regression after neoadjuvant immunotherapy compared to IPS^{High} patients (TRG1a/1b: IPS^{Low} = 50.0%, IPS^{High} = 15.4%; Fisher's exact test: $p = 0.015$; Fig. 4b and **c**). The Mann–Whitney test confirmed a lower IPS in patients with TRG 1a/1b ($p = 0.0009$; Fig. 4b). Simultaneously, we analyzed the radiological results. Among patients on IPS^{Low}, three patients had complete tumor disappearance (CR) and 14 patients had partial remission (PR), resulting in an objective response rate (ORR) of 68.0%, which was significantly better than the ORR of 25.9% among IPS^{High} patients (Fisher's exact test: $p = 0.009$; Fig. 4d and **Supplementary S11b**). In parallel, Kaplan–Meier survival analysis revealed that patients with IPS^{Low} had a lower postoperative recurrence rate and longer recurrence-free survival (RFS) than patients with IPS^{High} tumors (log-rank $p = 0.044$; Fig. 4e). In contrast, patients with IPS^{High} failed to exhibit changes before and after treatment. The χ^2 and fisher's exact tests indicated that patients with IPS^{Low} had lower ypT, ypN, and ypTNM stages after receiving neoadjuvant immunotherapy (**Table 1**).

However, patients receiving neoadjuvant ICI therapy also received chemotherapy, which may have biased the results; thus, we included 52 patients who received only the same neoadjuvant chemotherapy regimen as the controls (**Supplementary Fig. S10c** and **Supplementary Table S8**). Among all IPS^{Low} patients who received ICI therapy versus those receiving chemotherapy only, ICI therapy demonstrated a higher ORR, more significant tumor regression, and lower postoperative staging (ORR: nICI with nCT = 68.0%; nCT only = 42.3%; **Supplementary Table S9**). Although limited by a sample size that fell short of statistical significance, this trend of this result indicated that the predictive power of the IPS may be specific to neoadjuvant immunotherapy and independent of neoadjuvant chemotherapy. This further suggested that the IPS may remain applicable when anti-PD-1 therapy is co-applied with other therapies, such as different regimens of chemotherapy or molecular targeted therapies.

Patients with MSI-H or EBV are considered suitable for immunotherapy, yet there are still some non-MSI-H and non-EBV patients who could benefit from immunotherapy [36]. The results of the present study show that the IPS still identifies beneficiaries of neoadjuvant immunotherapy from MSS (ORR: IPS^{Low} = 65.2%, IPS^{High} = 24.0%; χ^2 test $p = 0.004$) and EBV-negative (ORR: IPS^{Low} = 65.2%, IPS^{High} = 26.9%; χ^2 test $p = 0.007$) patients (**Supplementary Fig. S11d-e**); thus, potential immunotherapy strategies for MSS and EBV-negative patients may be sought. In short, the IPS may not only be an alternative to MSI or EBV subtypes, but also a powerful complement to MSI and EBV subtypes in the application of immunotherapy. However, the limited sample of the nICI cohort, with only four patients with GC detected for MSI-H (7.7%) and three for EBV-positive (5.8%), limited further exploration.

Tumors with CPS ≥ 5 and the Inflamed phenotype are considered to be robust signs of a positive response to anti-PD-L1 treatment [37–39]; thus, the accuracy of the IPS with CPS and the Inflamed phenotype in predicting anti-PD-1 therapy was compared by plotting ROC curves. The results showed that the AUC of the IPS was significantly better than that of CPS and the Inflamed phenotype, regardless of whether the radiological response or TRG was used as the outcome (Fig. 4f and **g**). Univariate and multivariate logistic regression analysis also supported the strongly correlated IPS and immunotherapeutic response (Fig. 4h and **Supplementary S11f**). To attempt to confirm whether the

combination of IPS with CPS enhances the discrimination of the response to ICI therapy, patients were classified into four types according to the IPS with CPS. Interestingly, patients with Type A (IPS^{Low} with CPS ≥ 5) had an ORR of 84.6% and the ratio of TRG1a/1b of 61.5% and were the group most likely to benefit from ICI therapy, whereas Type D (IPS^{High} with CPS < 5) had an ORR of only 14.3% and the ratio of TRG1a/1b of 61.5% and these patients were considered unsuitable for ICI therapy (Fig. 4i and **Supplementary S11g**). Survival analysis also demonstrated that CPS combined with IPS more significantly differentiated the long-term prognosis of patients receiving neoadjuvant ICI therapy (**Supplementary Fig. S11h**). In addition, ineffective ICI therapy was observed in 47.4% of patients with CPS ≥ 5 and the Inflamed phenotype. These patients who failed to respond to ICI therapy had a higher IPS and significant upregulation of LAG-3 (**Supplementary Fig. 4j and S11i**). According to the results of this study, patients with the Inflamed phenotype did not respond to anti-PD-1 therapy as consistently as expected, and non-responders could still be observed in patients with both the Inflamed phenotype and PD-L1 dual positivity. Encouragingly, these non-responders could be identified by the IPS. Here, the association of the IPS with the Inflamed phenotype was identified, and it currently appears that IPS^{Low} potentially serves as an alternative to and beyond the Inflamed phenotype in neoadjuvant ICI therapy.

Overall, the IPS was outperformed as a powerful biomarker for predicting the response to ICI therapy by PD-L1 and the Inflamed phenotype. The combination of the IPS and CPS accurately identified immunotherapy-sensitive and -naïve patients. Additionally, overexpression of LAG-3 in non-responders with CPS > 5 and the Inflammatory phenotype was observed, which raised concern.

Discussion

Growing evidence supports the dominance of the TME in immunotherapy [40–42]; thus, accurate and efficient classification of the TME may be the key to advancing clinical individualized immunotherapy. In this study, based on screened immunophenotypic characteristics, an IPS applicable to pathological tissues for more efficient quantification and classification of the TME in the clinical process was developed. By evaluating the IPS, patients with GC were classified into two immune states: IPS^{Low} matched immune-activated, while IPS^{High} matched immune-silenced. These two immune states of patients with GC were distinctly different both in prognosis and responsiveness to ICI therapy, as supported by data from seven independent medical centers. Figure 5 illustrates the characteristics of the patients with different IPS derived from this study.

This promising performance of the IPS was attributed to the ability to separate the TME. In IPS^{Low} tumors, $CD8^+$ and $CD4^+$ T cells were abundantly recruited in the tumor parenchyma. Further analysis revealed that dense $GZMB^+CD8^+$ Teffs were present in the tumor-nest region of CT in IPS^{Low}, reflecting the advantage of the tumor-targeted migration ability of Teffs [43]. In addition, a high rate of M1 macrophages ($CD68^+INOS^+$) was observed in the tumor epithelium, which together with Teffs defined the hyperinflammatory microenvironment of IPS^{Low} tumors and a favorable outcome. These results suggest pre-existing antitumor immunity, which is a prerequisite for the efficacy of immunotherapy [33, 44, 45].

Although previous studies have reported an increase of immune checkpoints and Tregs in the inflammation-promoting environment through negative immune feedback [46, 47], the opposite trend of Tregs was observed in the present study, where Tregs appeared to be suppressed in the tumor core of IPS^{Low}, which seems to indicate a hypo-immunosuppressive profile of IPS^{Low}. As for immune checkpoints, coinciding with previous studies, IPS^{Low} tumors also showed enriched expression of immune checkpoints, which is a self-balancing of the immune system and not driven by tumor cells [47]. Therefore, the application of immunotherapy is expected to accelerate the immune effect to abrogate the tumor by disrupting this balance in the tumor parenchyma.

Neoadjuvant immunotherapy applied to resectable tumors had improved patient RFS and OS in several clinical trials. However, the known PD-L1, MSI status, EBV status, and TMB remain unstable in predicting the benefit of ICI therapy [36, 48]. To date, especially in GC, effective biomarkers to predict the responsiveness of neoadjuvant ICI therapy before treatment have remained absent. Excitingly, in this study, we revealed the predictive value of the IPS for neoadjuvant immunotherapy in GC, which could identify beneficiaries from non-MSI-H and EBV-negative subtypes. In parallel, the predictive abilities of the IPS for neoadjuvant ICI therapy were superior to and independent of the two accepted biomarkers PD-L1 (CPS) and CD8 (Inflamed phenotype). Moreover, the result of multivariate logistic regression indicated the potential of the IPS in combination with PD-L1. Patients with IPS^{Low} and CPS $\geq$ 5 were found to be the most beneficial to receiving neoadjuvant ICI therapy. In contrast, patients with IPS^{High} and CPS < 5 were non-responders to neoadjuvant ICI therapy and prone to postoperative relapse. Considering the potential immune-related adverse events, patients with IPS^{High} and CPS < 5 may be unsuitable for neoadjuvant ICI therapy.

PD-L1-rich and Inflamed tumors are considered sensitive to ICI therapy [37–39]; however, non-responders remain observable in these tumors. Interestingly, most of these non-responders exhibited a significantly elevated IPS, and further investigation revealed that the heightened IPS in these non-responders was driven by LAG-3 enrichment. Recent studies suggest that the antitumor effects of T cells with high expression of LAG-3 may fail to be rescued by a single PD-1/CTLA-4 blockade therapy [49, 50]. Based on this, we hypothesized that receiving a combination of LAG-3 with PD-1 blockade may be the key to reactivation of the antitumor effect in these patients (IPS^{High}, CPS $\geq$ 5, and Inflamed phenotype). Results from several clinical studies had revealed the clinical benefit and safety of anti-LAG-3 in combination with anti-PD-1 in the treatment of a variety of solid tumors [51–53], which drove the FDA to approve Opdualag, the first combination of LAG-3 with PD-1 blockade [54]. Meanwhile, the combination with relatlimab (anti-LAG-3) enhanced the effect of neoadjuvant anti-PD-1 therapy [55]. While these results are encouraging, the effectiveness of the LAG-3/PD-1 combination inhibitor remains limited in unselected patients [56], and robust biomarkers are required to identify patients who could potentially benefit. Compared to other TME-based signatures, the IPS incorporated the contribution of LAG-3, which may be a potential advantage of the IPS in predicting the combination of LAG-3 with PD-1 blockade therapy. Regrettably, we currently have no clinical evidence to confirm the value of the IPS in combination therapies, and a prospective, multicenter trial is needed to validate our conjecture.

The IPS differs from other TME-based signatures, not only for postoperative pathological specimens but also for biopsy specimens obtained preoperatively by gastroscopy, which facilitates the implementation of clinical translation. When patients are diagnosed with GC by biopsy tissue obtained by gastroscopy, only five indicators (WARS, UBE2L6, GZMB, BATF2, and LAG-3) of immunohistochemistry staining of the remaining biopsy tissue are sufficient to obtain the IPS to determine the strategy of neoadjuvant therapy, without other invasive additional examinations. Although the IPS holds significant clinical promise in GC, there were some limitations to this study. Firstly, this study was based on retrospective data and there might have been unaware bias in the selection of patients with GC. Secondly, the limited sample size (FMUUN-RNA_Seq Cohort) may have excluded some meaningful genes when selecting DEGs by confirming transcription-translation concordance. Finally, the number of patients in the neoadjuvant ICI therapy cohort remained low, and a higher number of individuals for both trial and control cohorts is necessary to reconfirm the results of this study further.

In summary, the IPS is a robust and stable signature applicable to pathological tissues to evaluate the prognosis and response to neoadjuvant ICI therapy in patients with GC by comprehensively classifying the TME (Fig. 5). Furthermore, the stratification of patients with GC by the IPS and CPS may be a valuable step towards more tailored and precise immunotherapy.

Abbreviations

AJCC
American Joint Committee on Cancer
ATA
Assessable Tumor Area
AUC
Area Under Curve
CPS
Combined Positive Score
CT
Core of Tumor
DEGs
Differentially Expressed Genes
EBV
the Epstein–Barr Virus
FFPE
Formalin-Fixed Paraffin-Embedded
GC
Gastric Cancer
GEO
Gene Expression Omnibus
HR

Hazard Ratio

ICI

Immune Checkpoint Inhibition

nICI

Neoadjuvant Immune Checkpoint Inhibition

IM

Invasive Margin

IPS

Immunophenotypic Score

LASSO

the Least Absolute Shrinkage and Selection Operator

MSI-H

Microsatellite Instability-High

MSS

Microsatellite Stability

ORR

Objective Response Rate

OR

Odd Ratio

OS

Overall Survival

RFS

Recurrence-Free Survival

ROC

Receiver Operating Characteristic Curve

ROI

Region of Interest

TAMs

Tumor Associated Macrophages

TCGA

The Cancer Genome Atlas

TME

Tumor Microenvironment

TRG

Tumor Regression Grade.

Declarations

Ethics approval and consent to participate

The ethics approval number for this research project is 2022KY084 and was obtained from the Fujian Medical University Union Hospital. All seven centers approved this study and all patients signed informed consent forms before tissue collection.

Consent for publication

Not applicable

Availability of data and material

The data supporting the findings in this study are available in the Article, Supplementary Information, or from the corresponding author upon reasonable request.

Competing interest

The authors have declared no conflicts of interest.

Funding

National Natural Science Foundation of China (No. 82173158, JBW)

National Youth Science Foundation Project of China (No. 81903080, LLC)

Natural Science Foundation of Fujian Province (No. 2021J06023, JBW)

Science and Technology Innovation Joint Fund Project of Fujian Province (No. 2019Y9089, CMH)

Construction Project of Fujian Province Minimally Invasive Medical Center (No. 2021662, CMH).

Author contributions

J.W. and Q.Q. conceived the study and drafted the manuscript. C.H. and C.Z. helped critically revise the manuscript for important intellectual content. Q.Q., Q.Z., and Y. Ye performed the research. Y.Yang, Y.Z., Y.X., T.Z., S.W., Q.W., and Q.J. provide the tissue samples from GC patients. P.L., J.Lin, J.Lu, Q.C., and L.C. helped collect data and design the study.

Acknowledgments

We thank the members of the Key Laboratory of the Ministry of Education for Gastrointestinal Cancer for their helpful comments and suggestions, and the Public Technology Service Center Fujian Medical University for their help and technical support.

References

1. Petricevic B, Kabiljo J, Zirnbauer R, Walczak H, Laengle J, Bergmann M: **Neoadjuvant immunotherapy in gastrointestinal cancers - The new standard of care?** *Seminars in cancer biology* 2022.
2. Eso Y, Seno H: **Current status of treatment with immune checkpoint inhibitors for gastrointestinal, hepatobiliary, and pancreatic cancers**. Therap Adv Gastroenterol 2020, **13**:1756284820948773.
3. Lee KW, Van Cutsem E, Bang YJ, Fuchs CS, Kudaba I, Garrido M, Chung HC, Lee J, Castro HR, Chao J *et al*: **Association of Tumor Mutational Burden with Efficacy of Pembrolizumab{plus minus}Chemotherapy as First-Line Therapy for Gastric Cancer in the Phase III KEYNOTE-062 Study**. Clin Cancer Res 2022.
4. Kang Y, Chen L, Ryu M, Oh D, Oh S, Chung H, Lee K, Omori T, Shitara K, Sakuramoto S *et al*: **Nivolumab plus chemotherapy versus placebo plus chemotherapy in patients with HER2-negative, untreated, unresectable advanced or recurrent gastric or gastro-oesophageal junction cancer (ATTRACTION-4): a randomised, multicentre, double-blind, placebo-controlled, phase 3 trial**. The Lancet Oncology 2022, **23**(2):234–247.
5. Shitara K, Ajani JA, Moehler M, Garrido M, Gallardo C, Shen L, Yamaguchi K, Wyrwicz L, Skoczylas T, Bragagnoli AC *et al*: **Nivolumab plus chemotherapy or ipilimumab in gastro-oesophageal cancer**. Nature 2022, **603**(7903):942–948.
6. Xu J, Jiang H, Pan Y, Gu K, Cang S, Han L, Shu Y, Li J, Zhao J, Pan H *et al*: **LBA53 Sintilimab plus chemotherapy (chemo) versus chemo as first-line treatment for advanced gastric or gastroesophageal junction (G/GEJ) adenocarcinoma (ORIENT-16): First results of a randomized, double-blind, phase III study**. Annals of Oncology 2021, **32**.
7. Ajani JA, D'Amico TA, Bentrem DJ, Chao J, Cooke D, Corvera C, Das P, Enzinger PC, Enzler T, Fanta P *et al*: **Gastric Cancer, Version 2.2022, NCCN Clinical Practice Guidelines in Oncology**. J Natl Compr Canc Netw 2022, **20**(2):167–192.
8. Topalian SL, Taube JM, Pardoll DM: **Neoadjuvant checkpoint blockade for cancer immunotherapy**. Science 2020, **367**(6477).
9. Andre T, Tougeron D, Piessen G, Fouchardiere CDL, Louvet C, Adenis A, Jary M, Tournigand C, Aparicio T, Desrame J *et al*: **Neoadjuvant nivolumab plus ipilimumab and adjuvant nivolumab in patients (pts) with localized microsatellite instability-high (MSI)/mismatch repair deficient (dMMR) oeso-gastric adenocarcinoma (OGA): The GERCOR NEONIPIGA phase II study**. Journal of Clinical Oncology 2022, **40**(4_suppl):244–244.
10. Cercek A, Lumish M, Sinopoli J, Weiss J, Shia J, Lamendola-Essel M, El Dika IH, Segal N, Shcherba M, Sugarman R *et al*: **PD-1 Blockade in Mismatch Repair-Deficient, Locally Advanced Rectal Cancer**. N Engl J Med 2022, **386**(25):2363–2376.
11. Huynh J, Patel K, Gong J, Cho M, Malla M, Parikh A, Klempner S: **Immunotherapy in Gastroesophageal Cancers: Current Evidence and Ongoing Trials**. Current treatment options in oncology 2021, **22**(11):100.
12. Hegde P, Karanikas V, Evers S: **The Where, the When, and the How of Immune Monitoring for Cancer Immunotherapies in the Era of Checkpoint Inhibition**. Clinical cancer research: an official journal of

the American Association for Cancer Research 2016, **22**(8):1865–1874.

13. Gajewski TF: **The Next Hurdle in Cancer Immunotherapy: Overcoming the Non-T-Cell-Inflamed Tumor Microenvironment**. Semin Oncol 2015, **42**(4):663–671.
14. Trujillo J, Sweis R, Bao R, Luke J: **T Cell-Inflamed versus Non-T Cell-Inflamed Tumors: A Conceptual Framework for Cancer Immunotherapy Drug Development and Combination Therapy Selection**. Cancer immunology research 2018, **6**(9):990–1000.
15. Durgeau A, Virk Y, Corgnac S, Mami-Chouaib F: **Recent Advances in Targeting CD8 T-Cell Immunity for More Effective Cancer Immunotherapy**. Front Immunol 2018, **9**:14.
16. Martinet L, Smyth MJ: **Balancing natural killer cell activation through paired receptors**. Nat Rev Immunol 2015, **15**(4):243–254.
17. Pardoll DM: **The blockade of immune checkpoints in cancer immunotherapy**. Nat Rev Cancer 2012, **12**(4):252–264.
18. Topalian SL, Hodi FS, Brahmer JR, Gettinger SN, Smith DC, McDermott DF, Powderly JD, Sosman JA, Atkins MB, Leming PD *et al*: **Five-Year Survival and Correlates Among Patients With Advanced Melanoma, Renal Cell Carcinoma, or Non-Small Cell Lung Cancer Treated With Nivolumab**. JAMA Oncol 2019, **5**(10):1411–1420.
19. Hamid O, Robert C, Daud A, Hodi FS, Hwu WJ, Kefford R, Wolchok JD, Hersey P, Joseph R, Weber JS *et al*: **Five-year survival outcomes for patients with advanced melanoma treated with pembrolizumab in KEYNOTE-001**. Ann Oncol 2019, **30**(4):582–588.
20. Ding QQ, Chauvin JM, Zarour HM: **Targeting novel inhibitory receptors in cancer immunotherapy**. Semin Immunol 2020, **49**:101436.
21. Zeng D, Li M, Zhou R, Zhang J, Sun H, Shi M, Bin J, Liao Y, Rao J, Liao W: **Tumor Microenvironment Characterization in Gastric Cancer Identifies Prognostic and Immunotherapeutically Relevant Gene Signatures**. Cancer immunology research 2019, **7**(5):737–750.
22. Gautier L, Cope L, Bolstad BM, Irizarry RA: **affy–analysis of Affymetrix GeneChip data at the probe level**. Bioinformatics 2004, **20**(3):307–315.
23. Lin J-L, Lin J-X, Lin JP, Zheng C-H, Li P, Xie J-W, Wang J-b, Lu J, Chen Q-Y, Huang C-M: **Safety and Efficacy of Camrelizumab in Combination With Nab-Paclitaxel Plus S-1 for the Treatment of Gastric Cancer With Serosal Invasion**. Frontiers in Immunology 2022, **12**.
24. Eisenhauer EA, Therasse P, Bogaerts J, Schwartz LH, Sargent D, Ford R, Dancey J, Arbuck S, Gwyther S, Mooney M *et al*: **New response evaluation criteria in solid tumours: revised RECIST guideline (version 1.1)**. Eur J Cancer 2009, **45**(2):228–247.
25. Becker K, Langer R, Reim D, Novotny A, Meyer zum Buschenfelde C, Engel J, Friess H, Hofler H: **Significance of histopathological tumor regression after neoadjuvant chemotherapy in gastric adenocarcinomas: a summary of 480 cases**. Ann Surg 2011, **253**(5):934–939.
26. Becker K, Mueller JD, Schulmacher C, Ott K, Fink U, Busch R, Böttcher K, Siewert JR, Höfler H: **Histomorphology and grading of regression in gastric carcinoma treated with neoadjuvant chemotherapy**. Cancer 2003, **98**(7):1521–1530.

27. Newman AM, Liu CL, Green MR, Gentles AJ, Feng W, Xu Y, Hoang CD, Diehn M, Alizadeh AA: **Robust enumeration of cell subsets from tissue expression profiles**. Nat Methods 2015, **12**(5):453–457.
28. Wilkerson MD, Hayes DN: **ConsensusClusterPlus: a class discovery tool with confidence assessments and item tracking**. Bioinformatics 2010, **26**(12):1572–1573.
29. Ritchie ME, Phipson B, Wu D, Hu Y, Law CW, Shi W, Smyth GK: **limma powers differential expression analyses for RNA-sequencing and microarray studies**. Nucleic Acids Res 2015, **43**(7):e47.
30. Ganesh K, Stadler ZK, Cercek A, Mendelsohn RB, Shia J, Segal NH, Diaz LA, Jr.: **Immunotherapy in colorectal cancer: rationale, challenges and potential**. Nat Rev Gastroenterol Hepatol 2019, **16**(6):361–375.
31. Xie T, Liu Y, Zhang Z, Zhang X, Gong J, Qi C, Li J, Shen L, Peng Z: **Positive Status of Epstein-Barr Virus as a Biomarker for Gastric Cancer Immunotherapy: A Prospective Observational Study**. J Immunother 2020, **43**(4):139–144.
32. Goc J, Germain C, Vo-Bourgais TK, Lupo A, Klein C, Knockaert S, de Chaisemartin L, Ouakrim H, Becht E, Alifano M *et al*: **Dendritic cells in tumor-associated tertiary lymphoid structures signal a Th1 cytotoxic immune contexture and license the positive prognostic value of infiltrating CD8 + T cells**. Cancer Res 2014, **74**(3):705–715.
33. Tumeh P, Harview C, Yearley J, Shintaku I, Taylor E, Robert L, Chmielowski B, Spasic M, Henry G, Ciobanu V *et al*: **PD-1 blockade induces responses by inhibiting adaptive immune resistance**. Nature 2014, **515**(7528):568–571.
34. Gros A, Robbins PF, Yao X, Li YF, Turcotte S, Tran E, Wunderlich JR, Mixon A, Farid S, Dudley ME *et al*: **PD-1 identifies the patient-specific CD8â□º tumor-reactive repertoire infiltrating human tumors**. J Clin Invest 2014, **124**(5):2246–2259.
35. Bruni D, Angell HK, Galon J: **The immune contexture and Immunoscore in cancer prognosis and therapeutic efficacy**. Nat Rev Cancer 2020, **20**(11):662–680.
36. Panda A, Mehnert JM, Hirshfield KM, Riedlinger G, Damare S, Saunders T, Kane M, Sokol L, Stein MN, Poplin E *et al*: **Immune Activation and Benefit From Avelumab in EBV-Positive Gastric Cancer**. J Natl Cancer Inst 2018, **110**(3):316–320.
37. Cristescu R, Mogg R, Ayers M, Albright A, Murphy E, Yearley J, Sher X, Liu XQ, Lu H, Nebozhyn M *et al*: **Pan-tumor genomic biomarkers for PD-1 checkpoint blockade-based immunotherapy**. Science 2018, **362**(6411).
38. Tang H, Wang Y, Chlewicki LK, Zhang Y, Guo J, Liang W, Wang J, Wang X, Fu YX: **Facilitating T Cell Infiltration in Tumor Microenvironment Overcomes Resistance to PD-L1 Blockade**. Cancer Cell 2016, **29**(3):285–296.
39. Galon J, Bruni D: **Approaches to treat immune hot, altered and cold tumours with combination immunotherapies**. Nature reviews Drug discovery 2019, **18**(3):197–218.
40. Chen DS, Mellman I: **Elements of cancer immunity and the cancer–immune set point**. Nature 2017, **541**(7637):321–330.

41. Hegde PS, Karanikas V, Evers S: **The Where, the When, and the How of Immune Monitoring for Cancer Immunotherapies in the Era of Checkpoint Inhibition**. Clin Cancer Res 2016, **22**(8):1865–1874.
42. Nishino M, Ramaiya NH, Hatabu H, Hodi FS: **Monitoring immune-checkpoint blockade: response evaluation and biomarker development**. Nat Rev Clin Oncol 2017, **14**(11):655–668.
43. Duckworth BC, Qin RZ, Groom JR: **Spatial determinates of effector and memory CD8(+) T cell fates**. Immunol Rev 2022, **306**(1):76–92.
44. Herbst RS, Soria JC, Kowanetz M, Fine GD, Hamid O, Gordon MS, Sosman JA, McDermott DF, Powderly JD, Gettinger SN *et al*: **Predictive correlates of response to the anti-PD-L1 antibody MPDL3280A in cancer patients**. Nature 2014, **515**(7528):563–567.
45. Harlin H, Meng Y, Peterson AC, Zha Y, Tretiakova M, Slingluff C, McKee M, Gajewski TF: **Chemokine expression in melanoma metastases associated with CD8 + T-cell recruitment**. Cancer Res 2009, **69**(7):3077–3085.
46. Chen DS, Mellman I: **Elements of cancer immunity and the cancer-immune set point**. Nature 2017, **541**(7637):321–330.
47. Spranger S, Spaapen RM, Zha Y, Williams J, Meng Y, Ha TT, Gajewski TF: **Up-regulation of PD-L1, IDO, and T(regs) in the melanoma tumor microenvironment is driven by CD8(+) T cells**. Sci Transl Med 2013, **5**(200):200ra116.
48. Fuchs CS, Doi T, Jang RW, Muro K, Satoh T, Machado M, Sun W, Jalal SI, Shah MA, Metges JP *et al*: **Safety and Efficacy of Pembrolizumab Monotherapy in Patients With Previously Treated Advanced Gastric and Gastroesophageal Junction Cancer: Phase 2 Clinical KEYNOTE-059 Trial**. JAMA Oncol 2018, **4**(5):e180013.
49. Shen R, Postow MA, Adamow M, Arora A, Hannum M, Maher C, Wong P, Curran MA, Hollmann TJ, Jia L *et al*: **LAG-3 expression on peripheral blood cells identifies patients with poorer outcomes after immune checkpoint blockade**. Sci Transl Med 2021, **13**(608).
50. Mimura K, Kua LF, Xiao JF, Asuncion BR, Nakayama Y, Syn N, Fazreen Z, Soong R, Kono K, Yong WP: **Combined inhibition of PD-1/PD-L1, Lag-3, and Tim-3 axes augments antitumor immunity in gastric cancer-T cell coculture models**. Gastric Cancer 2021, **24**(3):611–623.
51. Garralda E, Sukari A, Lakhani N, Patnaik A, Lou Y, Im S-A, Golan T, Geva R, Wermke M, Miguel M *et al*: **A phase 1 first-in-human study of the anti-LAG-3 antibody MK4280 (favezelimab) plus pembrolizumab in previously treated, advanced microsatellite stable colorectal cancer**. Journal of Clinical Oncology 2021, **39**:3584–3584.
52. Hamid O, Wang D, Kim T, Kim S-W, Lakhani N, Johnson M, Groisberg R, Papadopoulos K, Kaczmar J, Middleton M *et al*: **Clinical activity of fianlimab (REGN3767), a human anti-LAG-3 monoclonal antibody, combined with cemiplimab (anti-PD-1) in patients (pts) with advanced melanoma**. Journal of Clinical Oncology 2021, **39**:9515–9515.
53. Tawbi HA, Schadendorf D, Lipson EJ, Ascierto PA, Matamala L, Castillo Gutiérrez E, Rutkowski P, Gogas HJ, Lao CD, De Menezes JJ *et al*: **Relatlimab and Nivolumab versus Nivolumab in Untreated Advanced Melanoma**. N Engl J Med 2022, **386**(1):24–34.

54. Paik J: **Nivolumab Plus Relatlimab: First Approval**. Drugs 2022, **82**(8):925–931.
55. Amaria R, Postow M, Tetzlaff M, Ross M, Glitza I, McQuade J, Wong M, Gershenwald J, Goepfert R, Keung E *et al*: **Neoadjuvant and adjuvant nivolumab (nivo) with anti-LAG3 antibody relatlimab (rela) for patients (pts) with resectable clinical stage III melanoma**. Journal of Clinical Oncology 2021, **39**:9502–9502.
56. Ascierto P, Melero I, Bhatia S, Bono P, Sanborn R, Lipson E, Callahan M, Gajewski T, Gomez-Roca C, Hodi F *et al*: **Initial efficacy of anti-lymphocyte activation gene-3 (anti–LAG-3; BMS-986016) in combination with nivolumab (nivo) in pts with melanoma (MEL) previously treated with anti–PD-1/PD-L1 therapy**. Journal of Clinical Oncology 2017, **35**:9520–9520.

Tables

Table 1 is available in the Supplementary Files section.

Figures

Figure 1

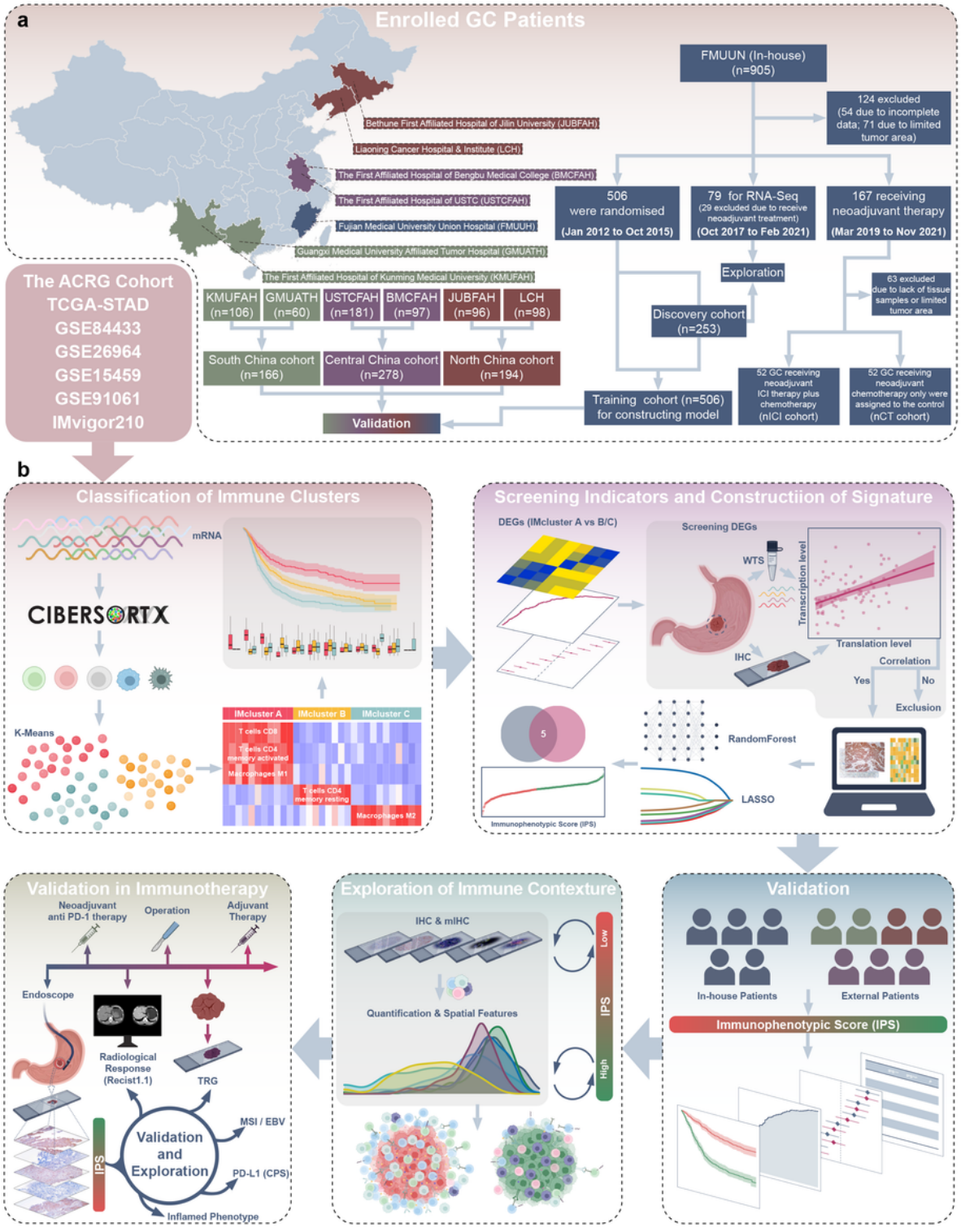

Figure 1

The overall design of the study. GC, Gastric Cancer; DEGs, Differentially Expressed Genes; WTS, Whole-Transcriptome Sequencing; IHC, Immunohistochemistry; IPS, Immunophenotypic Score; mIHC, Multiplex Immunohistochemistry Staining; TRG, Tumor Regression Grade; CPS, Combined Positive Score .

Figure 2

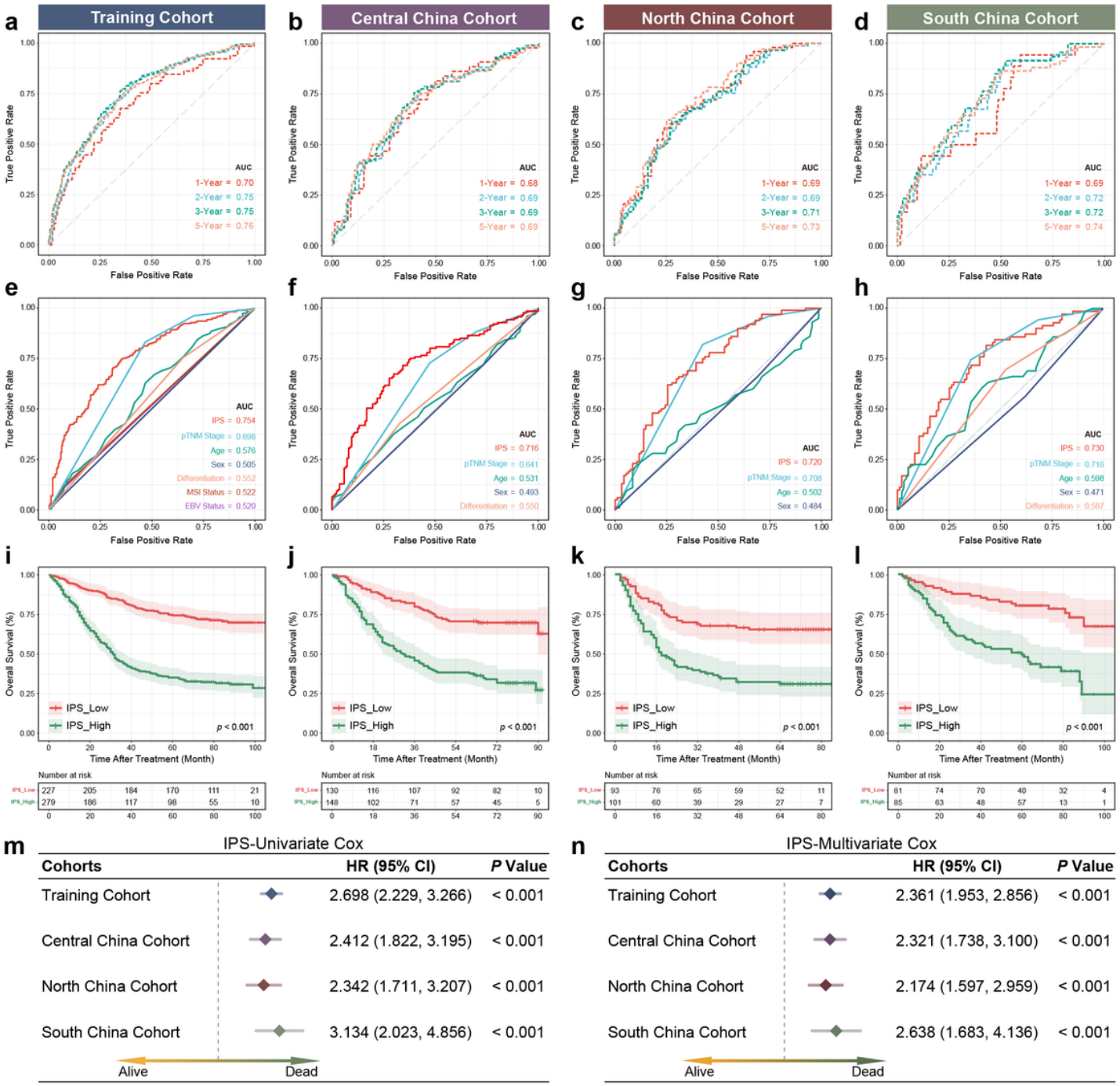

Figure 2

Data from four cohorts consisting of seven independent medical centers confirm the prognostic value of IPS for GC (**a**–**d**) Time-dependent ROC curves of four cohorts demonstrate the accuracy and stability of IPS in predicting the prognosis. (**e**–**h**) Comparison of the prognostic value of the IPS versus clinicopathological features in four cohorts by ROC curves. (**i**–**l**) Kaplan–Meier curves for OS according to the IPS in four cohorts (log-rank test, all $p < 0.001$). (**m**–**n**) Univariate and multivariate Cox regression analysis was performed to explore the prognostic value of IPS (all $p < 0.001$). Variables with statistical significance in the univariate analysis were integrated into the multivariate analysis. The dotted line

represents the hazard ratio (HR) = 1. Training Cohort: n = 506, Central China Cohort: n = 178, North China Cohort: n = 194, South China Cohort: n = 166.

Figure 3

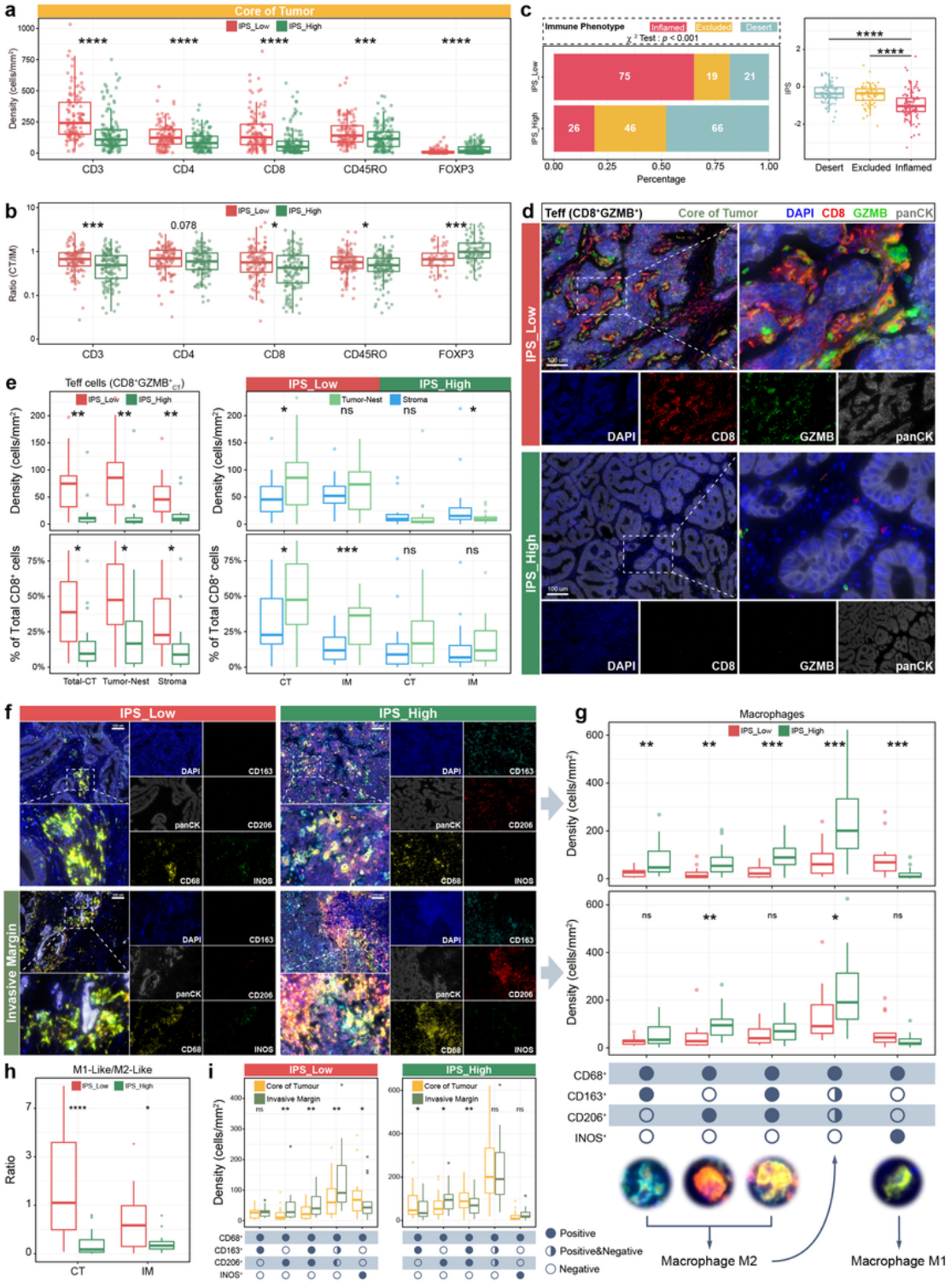

Figure 3

IPS-specific landscape of the tumor immune microenvironment (**a**) Comparison of immune infiltration in the core of tumor (CT; $CD3^+$, $CD4^+$, $CD8^+$, $CD45RO^+$, and $FOXP3^+$) between the IPS^{Low} and IPS^{High} in the

Discovery Cohort (n = 253). ***$p < 0.001$; ****$p < 0.0001$, Mann–Whitney U test. (**b**) Comparing the ratio of immune cell infiltration ($CD3^+$, $CD4^+$, $CD8^+$, $CD45RO^+$, and $FOXP3^+$) in the CT to the invasive margin (IM) between the IPS^{Low} and IPS^{High}. Cases with density < 5 cells/mm^2 were excluded to reduce the abnormal oversize/undersize ratio ($CD3^+$: n = 251, $CD4^+$: n = 244, $CD8^+$: n = 239, $CD45RO^+$: n = 249, $FOXP3^+$: n = 130). *$p < 0.05$; ***$p < 0.001$, Mann–Whitney U-test. (**c**) Components of the immunophenotypes (Inflamed, Excluded, and Desert) of IPS^{Low} versus IPS^{High} ($p < 0.001$, χ^2 test), while comparing the IPS between the three immunophenotypes. ****$p < 0.0001$, Mann–Whitney U-test. (**d**) Multiplexed immunohistochemical staining was used to visualize the effector T cells (Teffs; $GZMB^+CD8^+$) in the CT of IPS^{Low} vs IPS^{High}, and $panCK^+$ was used to segment the tumor-nest and stroma (n = 32; scale bar = 100 μm). (**e**) Comparison of the density and ratio (to total CD8+ cells) of Teffs in the CT between IPS^{Low} and IPS^{High} (Mann–Whitney U-test), and the distribution characteristics of Teffs in different locations of the tumor-nest and stroma (Wilcoxon matched-pairs signed rank test). *$p < 0.05$; **$p < 0.01$; ***$p < 0.001$. (**f**) Multiplex immunofluorescence staining characterized the macrophage infiltration profile of IPS^{Low} and IPS^{High} in the CT and IM (CD68-yellow, CD163-cyan, CD206-red, INOS-green, panCK-grey, and DAPI-blue; n = 32; scale bar = 100 μm). (**g**) Comparison of the density of different macrophage subtypes between IPS^{Low} and IPS^{High} in the CT (upper panel) and IM (lower panel). The red dotted line represents the margin between tumor and normal tissue. *$p < 0.05$; **$p< 0.01$; ***$p < 0.001$; ****$p < 0.0001$, Mann–Whitney U-test. (**h**) Differences in the ratio of M1 to M2 macrophages in IPS^{Low} vs IPS^{High}. > 1 means more M1-like, < 1 means more M2-like. *$p < 0.05$; ****$p < 0.0001$, Mann–Whitney U-test. (**i**) Distribution tendency of different macrophage subsets in IPS^{Low} and IPS^{High} tumors. *$p < 0.05$; **$p < 0.01$, Wilcoxon matched-pairs signed rank test.

Figure 4

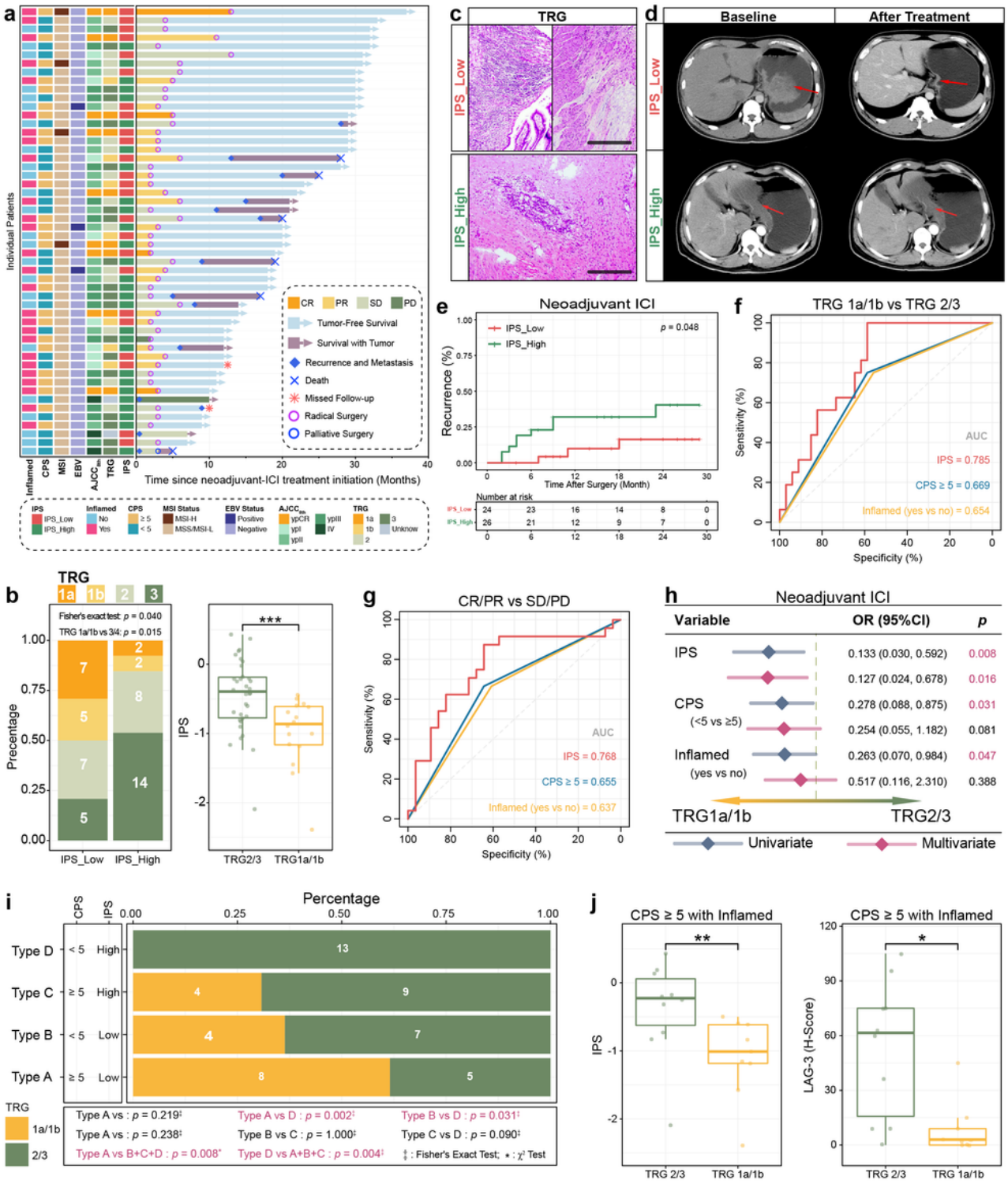

Figure 4

IPS accurately predicts the neoadjuvant ICI therapy response (**a**) Overview of treatment for patients with locally advanced GC receiving neoadjuvant ICI therapy (n = 52). (**b**) Composition of TRG to neoadjuvant ICI therapy in IPS^{Low} versus IPS^{High} (p = 0.040, Fisher's exact test). Meanwhile, the IPS was compared between TRG 1a/1b and TRG 3/4 patients (p < 0.001, Mann–Whitney U-test). (**c**) Postoperative pathological tissue images of no. 40 (upper panel, IPS^{Low}) and no. 47 (lower panel, IPS^{High}). Patient no.

40 had a completely regressed tumor (TRG1a), while patient no. 47 still had a residual tumor (TRG 3). Scale bar = 50 μm. (**d**) CT imaging changed before and after neoadjuvant ICI therapy in patient no. 40 (IPS^{Low}) and patient no. 47 (IPS^{High}). (**e**) Kaplan–Meier survival analysis demonstrated recurrence in IPS^{Low} vs IPS^{High} patients ($p = 0.048$, log-rank test). (**f** and **g**) Comparing the accuracy of biomarkers (IPS, CPS, and Inflamed phenotype) in predicting the response to neoadjuvant ICI therapy by ROC curves. (**h**) Univariate and multivariate logistic regression analysis to confirm the value of biomarkers (IPS, CPS, and Inflamed phenotype) for predicting neoadjuvant ICI therapy (outcome: TRG1a/1b). OR: Odd Ratio. (**i**) Comparison of the TRG to neoadjuvant ICI therapy across Type A (IPS^{Low} with CPS ≥ 5), Type B (IPS^{Low} with CPS < 5), Type C (IPS^{High} with CPS ≥ 5), and Type D (IPS^{High} with CPS < 5). (**j**) Comparison of IPS and LAG-3 in TRG1a/1b and TRG2/3 patients with GC with CPS ≥ 5 and Inflamed phenotype (n = 19). ***$p < 0.001$, Mann–Whitney U-test.

Figure 5

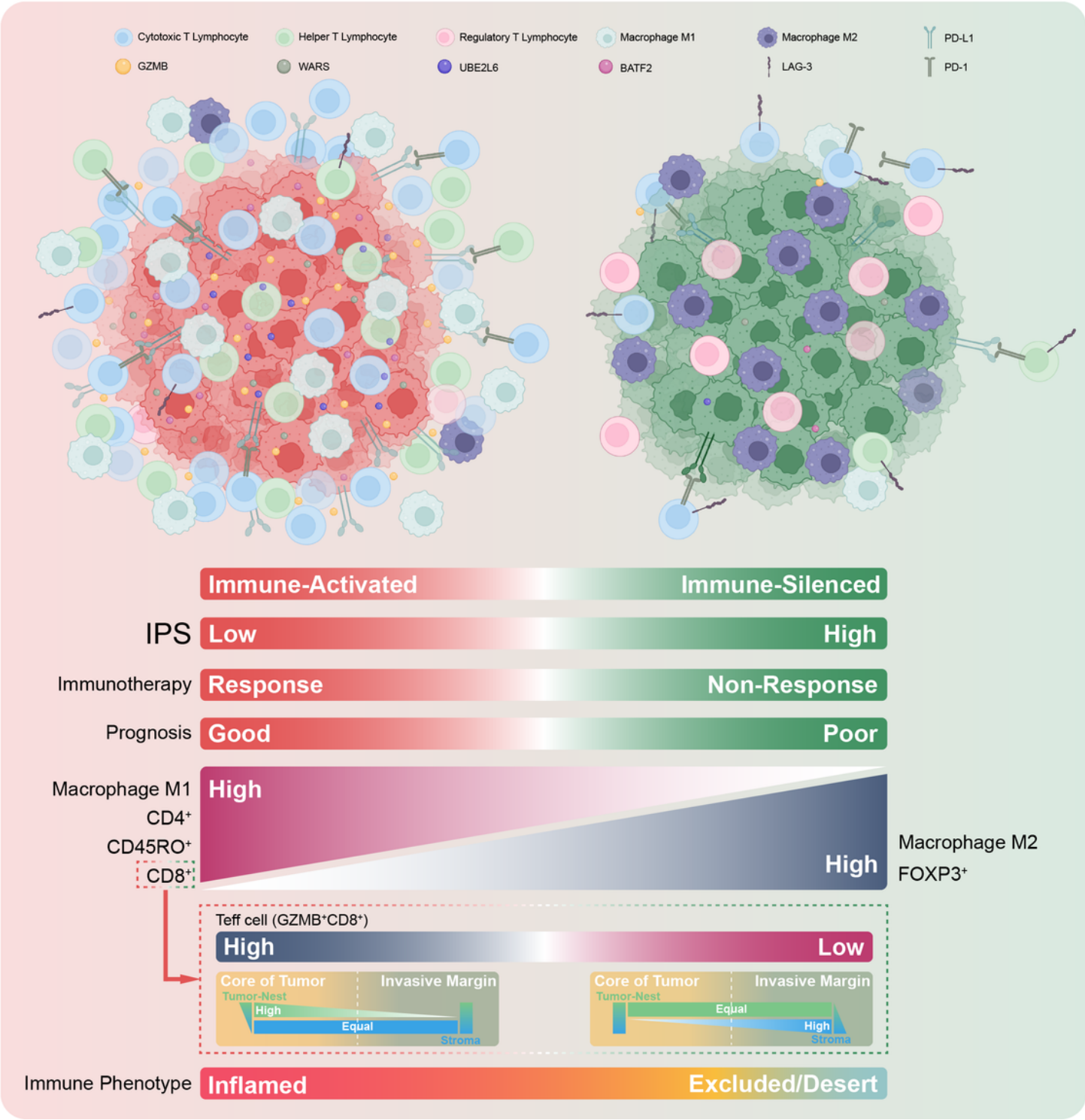

Figure 5

Schematic illustration of the characteristics associated with the immunophenotype score (IPS) in this study.

Supplementary Files

This is a list of supplementary files associated with this preprint. Click to download.

- Table1.pdf
- SupplementaryMaterials.pdf